

### §3. Optimization of Magnetic Configuration for the High Fusion Triple Product Operation

Miyazawa, J., Sakamoto, R., Goto, M., Morisaki, T., Motojima, G., Yamada, H.

High fusion triple product of  $n_{e0}\tau_E T_{e0} \sim 0.5 \times 10^{20} \text{ m}^{-3} \text{ s keV}$ , where  $n_{e0}$ ,  $\tau_E$  and  $T_{e0}$  are the central electron density, the energy confinement time, and the central electron temperature, respectively, has been achieved after finding of the high-density internal diffusion barrier (IDB) plasmas in LHD.<sup>1)</sup> There is an optimum magnetic configuration for  $n_{e0}\tau_E T_{e0} = p_{e0}\tau_E$ , where  $p_{e0} = n_{e0}T_{e0}$  is the central electron pressure, because of the opposite magnetic configuration dependence of  $p_{e0}$  and  $\tau_E$ .

Contrastive to the strong magnetic configuration dependence of the global energy confinement property in LHD,  $p_{e0}$  in pellet-fuelled plasmas including IDB plasmas increases with the central density in a similar manner at various magnetic configurations of  $R_{ax} = 3.60 - 3.80 \text{ m}$  as is shown in Fig. 1, where  $R_{ax}$  is the major radius of the magnetic axis in the vacuum condition. Nevertheless, the upper envelope of Fig. 1 suggests gyro-Bohm like density dependence of the pressure, *i.e.*,  $p_{e0} \propto n_{e0}^{0.6}$ , as is also observed for  $\tau_E$ .

$R_{ax}$  dependence of pellet-fuelled plasmas is summarized in Fig. 2, where the magnetic field strength and the heating power are fixed while the pellet injection scheme is optimized at each configuration.  $n_{e0}$  and  $p_{e0}$  increase as  $R_{ax}$  is shifted outward, while  $\tau_E$  monotonically decreases with increasing  $R_{ax}$ . In the case of Fig. 2, the optimum  $R_{ax}$  for high  $n_{e0}\tau_E T_{e0}$  is  $3.75 - 3.80 \text{ m}$ .

To achieve high  $n_{e0}\tau_E T_{e0}$ , it is effective to reduce the heating power after the IDB formation, which we call “annealing operation” on the analogy of metallurgy.<sup>1)</sup>  $n_{e0}\tau_E$  in various configurations is plotted as a function of  $T_{e0}$  in Fig. 3. The annealing operation has been carried out at  $R_{ax}$

= 3.70, 3.75, and 3.80 m. High  $n_{e0}\tau_E T_{e0}$  of  $\sim 0.5 \times 10^{20} \text{ m}^{-3} \text{ s keV}$  has been achieved in these configurations around  $R_{ax} \sim 3.75 \text{ m}$ , which are the optimum for high  $n_{e0}\tau_E T_{e0}$  as expected from the opposite tendency of  $p_{e0}$  and  $\tau_E$ .

1) Miyazawa, J., et al.: Ann. Rep. NIFS Apr. 2007 – Mar. 2008 (2008) 8

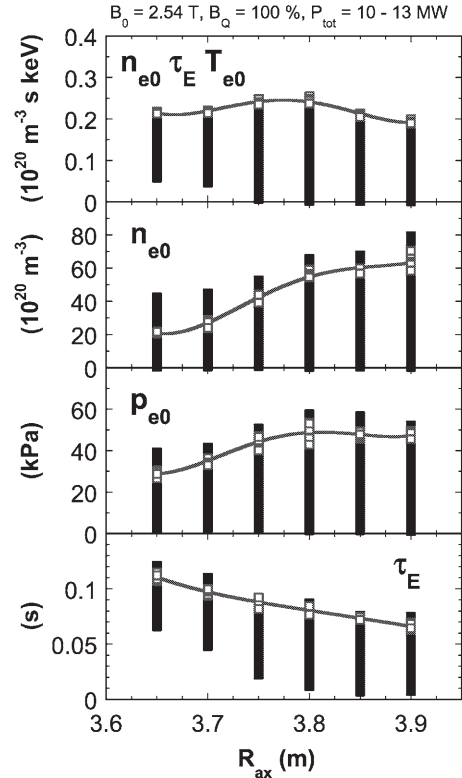


Fig. 2. Magnetic configuration dependence of  $n_{e0}\tau_E T_{e0}$ . The magnetic field strength of 2.54 T and the NB heating power of 10 – 13 MW are fixed. Open squares denote the subset of high  $n_{e0}\tau_E T_{e0}$ .

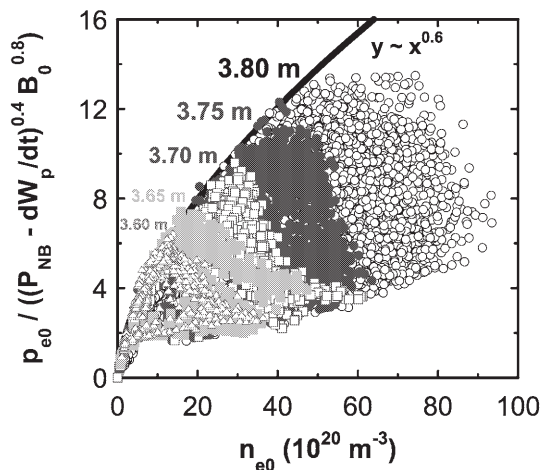


Fig. 1.  $n_{e0}$  dependence of  $p_{e0}$  normalized by the gyro-Bohm type parameter dependence in pellet-fuelled plasmas. The upper envelope suggests no or weak configuration dependence of  $p_{e0}$ , while the gyro-Bohm property is maintained.

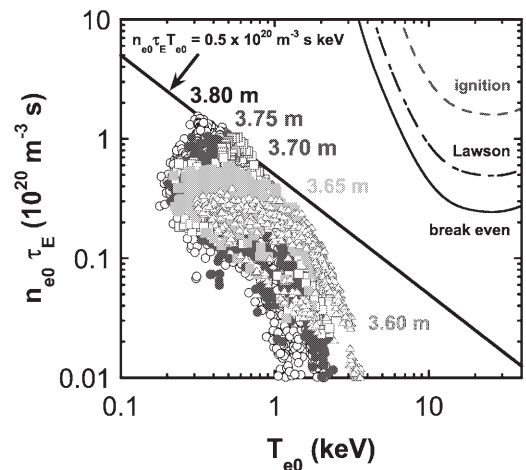


Fig. 3.  $T_{e0}$  dependence of  $n_{e0}\tau_E$  in various magnetic configurations. Important milestones to the fusion reactor of the break even condition, the Lawson condition, and the ignition condition are also depicted.